Resin-gel High incorporation of high concentrations W^{6+} and Zn^{2+} into TiO_2-Anatase crystal to form quaternary mixed-metal oxides: Effect on the a lattice parameter and photodegradation efficiency

Lerato Hlekelele*[a,b,c], Shane H. Durbach[a,b], Vongani P. Chauke[c], Farai Dziike[a,b], Paul J. Franklyn[a]

[a]Molecular Science Institute, School of Chemistry, University of the Witwatersrand, Johannesburg, 2050, South Africa

[b]DST-NRF Centre of Excellence in Strong Materials, University of the Witwatersrand, WITS, 2050, Johannesburg, South Africa

[c]Polymers and Composites, Materials Science and Manufacturing, Council for Scientific and Industrial Research, P.O Box 395, 0001, Pretoria, South Africa

E-mail: LHlekelele@csir.co.za

(S1) Sample composition

Table S1 Sample names and calcination temperatures applied for the concentration study of the various QMMOs.

Sample name	% Ti^{4+}	% W^{6+}	Zn^{2+}	Calcination temperature
TiO_2	100	0	0	400
WO_3	0	100	0	400
ZnO	0	0	100	400
TWZ910	90	10	0	400
TWZ901	90	0	10	400
TWZ820	80	20	0	400
TWZ811	80	10	10	400
TWZ802	80	0	20	400
TWZ730	70	30	0	400
TWZ721	70	20	10	400
TWZ712	70	10	20	400
TWZ703	70	0	30	400

(S2) Photodegradation testing

Slurry consisting of 25 mg of the materials and a BPA solution (50 ml, 60 ppm) was first magnetically stirred for 2 h in the dark to ensure adsorption equilibrium. Each mixture was then exposed to light for 60 min with a solar simulator. The photocatalytic experiments were conducted using visible light, where a UV-light filter ($\lambda > 400$ nm) was used. The light used was supplied using a 300 W Xenon Short Arc lamp (Eurolux). The lamp was placed 20 cm away from the sample to deliver radiation of 1000 W/m^2 measured using a monocrystalline

silicon photovoltaic cell. The reaction was carried out in an 80 ml quartz glass vessel. Periodically, during the photodegradation experiments, 1 ml aliquots were sampled and analyzed by high-performance liquid chromatography (HPLC) coupled with a photodiode array detector (UltiMate 3000). The analyte was eluted using a gradient method described in our previous work on a Phenomenex LUNA 5 mm C18 reversed-phase column.[1,2] The concentration of BPA was measured at 225 nm.

(S3) PXRD analyses of pure metal oxides

PXRD analyses were performed in order to study the crystallographic structure of the pure metal oxides and the mixed metal oxides. The PXRD patterns of the calcined pure metals oxides, i.e. TiO_2, ZnO, and WO_3 are shown in Fig. S1. It was deduced from the PXRD of ZnO that the material was exclusively hexagonal wurtzite (Zincite, JCPDS 5-0664), with reflections at 2θ positions of 37.136; 40.069; 42.566; 56.102; 66,949, 74.655; 78.933; 80.971 and 82.322°, indexed as (100), (002), (101), (102), (110), (103), (200), (112) and (201). There are no other peaks observed which were not accounted for, indicating that the procedure yielded pure ZnO.

In the case of WO_3, a series of peaks, some of which were overlapping were observed on its PXRD pattern. The peaks are generally narrow and strong which was attributed to that the materials were highly crystalline and had fairly big particles. The main peaks at 2θ positions: 16.340; 26.967; 28.763; 32.153; 32.831; 33.509; 40.069; 43.001; 48.882; 58.813; and 65.831 °, were indexed as: (100), (001), (110), (101), (200), (111), (201), (300), (002), (220), (202), (221) and (400) respectively (PDF card, 75-2187). All the diffraction peaks are that of hexagonal WO_3, indicating that the material synthesized is pure.
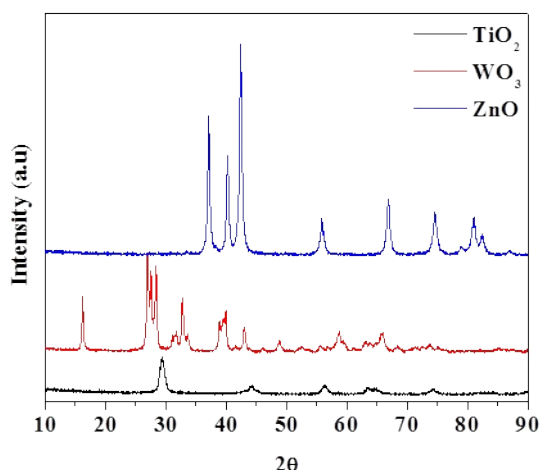
Fig. S1. PXRD patterns of TiO_2, WO_3, and ZnO.

On the other hand, The PXRD of TiO_2 has a series of peaks at 29.441; 44.356; 55.340; 63.797, 64.915; 74.286; 82.185; 83.568 and 86.247 °, indexed as: (101), (004), (200), (105), (211), (204), (116), (220) and (215), and as it is the case with ZnO and WO_3, all the peaks were accounted for indicating that the synthesized material is pure TiO_2 anatase.

(S4) TEM and EDS analyses of pure metal oxides

The pure metal oxides and the QMMOs were then analyzed by EDS to determine their elemental composition. TEM was used in order to study their morphological properties and particle size distribution. Here it was observed that the WO_3 nanoparticles are predominantly hexagonal (Fig. S2a and Fig. S2b), which is consistent with the PXRD analyses (Fig. S1). The particle size of the WO_3 nanoparticles ranged between 45 and 75 nm, with an average size of 55 nm as determined from TEM micrographs (Fig. S2b). EDS conducted on the particle shown in Fig. S2d showed that the material consisted of tungsten and oxygen (Fig. S2c). The copper peaks were present on the spectrum because a copper grid was used for specimen preparation (Fig. S2c).
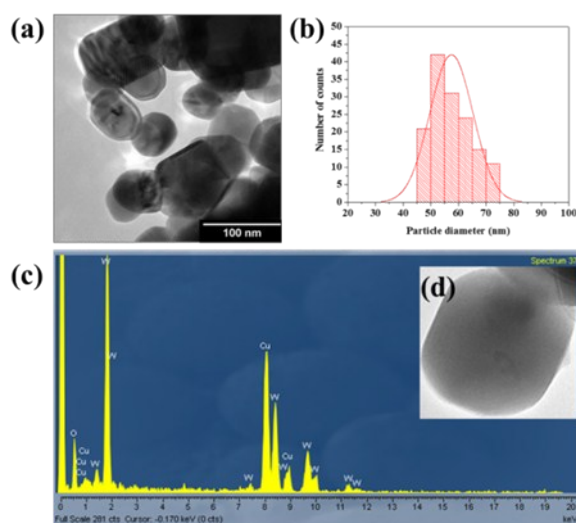
Fig. S2 (a) TEM image of WO_3, (b) WO_3 particle size distribution, (c) EDS spectra of WO_3 nanoparticles and (d) TEM image of particle which the EDS spectra was recorded on.

In the case of the ZnO sample, its morphology was found to inhomogeneous where some particles were found to be spherical and hexagonal in shape, whereas others had irregular facets (Fig. S3a). The diameter distribution of these particles ranged between 70-100 nm whilst most had a diameter of 85 nm as was determined from TEM micrographs by measuring *ca*. 100 particles from different images (Fig. S3b). As was the case with WO_3 nanoparticles, the EDS spectrum of ZnO (Fig. S3c) conducted on the particle shown in Fig. S3d showed that the material consisted of only Zn and O. A small carbon peak was also observed, which was attributed to carbon soot that resisted the annealing/calcination step.
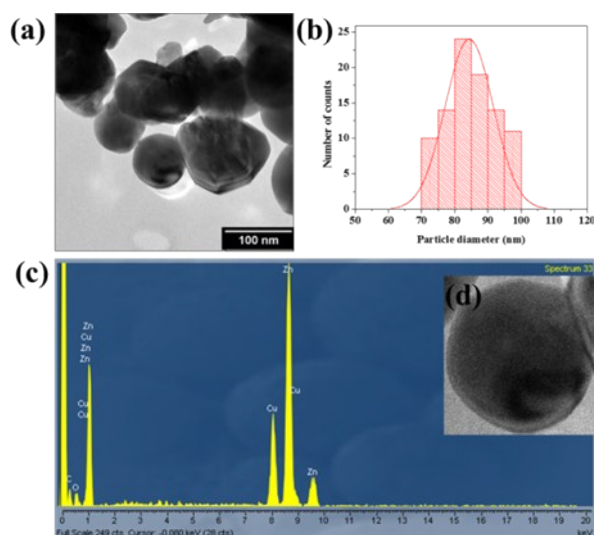
Fig. S3 (a) TEM image of ZnO, (b) ZnO particle size distribution, (c) EDS spectra of ZnO nanoparticles and (d) TEM image of particle which the EDS spectra was recorded on.

The morphological properties of TiO$_2$ nanoparticles were also studied by TEM. It was observed from the TEM images of TiO$_2$ nanoparticles that the sample consisted mostly of grain-like nanoparticles (Fig. S4a). These particles had sizes that ranged between 8 nm to 15 nm but were predominantly 11 nm (Fig. S4b). The EDS spectrum of TiO$_2$ (Fig. S4c) recorded on the particle shown in Fig. S4d showed that the material consisted of only Ti and O atoms, while a carbon peak was also observed. The carbon peak observed was due to the unburned carbon during the combustion and subsequent calcination process. Therefore, it was demonstrated by PXRD, laser Raman spectroscopy, TEM and EDS that the resin gel method is a viable method for the synthesis of pure metal oxides.
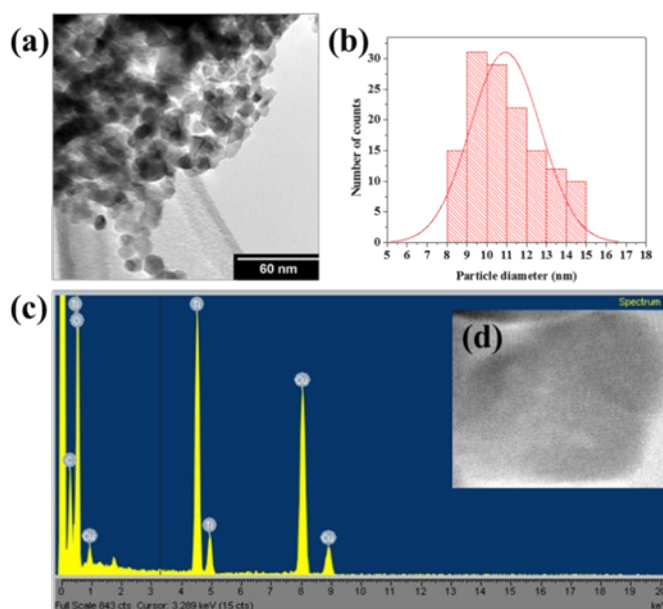
Fig. S4 (a) TEM image of TiO$_2$, (b) TiO$_2$ particle size distribution, (c) EDS spectra of TiO$_2$ nanoparticles and (d) TEM image of particle which the EDS spectra was recorded on.

(S5) Laser Raman spectroscopy

Laser Raman spectroscopy analyses were conducted in order to confirm what was observed from the PXRD patterns of the various pure metal oxides. The laser Raman spectrum of ZnO nanoparticles (**Fig. S5a and Fig. S5b** was observed to have been dominated by the two intense E_2 modes at 108 and 438 cm^{-1}. In addition, two more peaks were observed at 376 and 582 cm^{-1} which corresponded to the A_1 and E_1 symmetry modes of ZnO. As was the case with PXRD data, the laser Raman spectrum showed that the material was pure wurtzite.
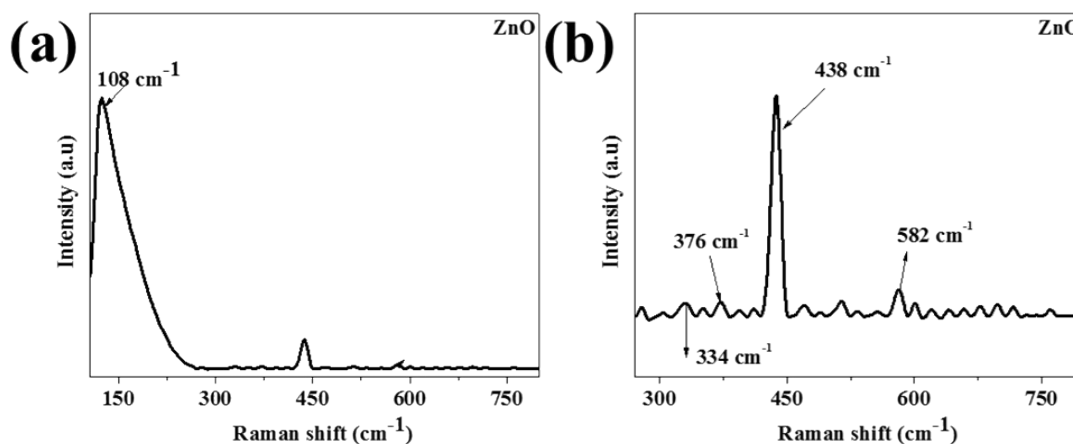
Fig. S5 Laser Raman spectrum of (**a**) ZnO and (**b**) expansion of the laser Raman spectrum of ZnO to show the low-intensity peaks.

Laser Raman spectroscopy was also used to confirm that pure WO_3 was synthesized using the resin gel synthesis. Several peaks were observed on the laser Raman spectrum of WO_3, which were all accounted for, thus further confirming that the material synthesized was indeed pure hexagonal WO_3 (**Fig. S6**). The peaks observed at 131 and 194 cm^{-1} were attributed to the lattice vibration modes. The peak at 260 and 326 cm^{-1} were attributed to the $W^{6+}=O$ stretching vibrations. The peak observed at 702 cm^{-1} was attributed to the asymmetric stretching vibration of W-O-W whereas that which was observed at 803 cm^{-1} was attributed to the symmetry stretching of the same bond.
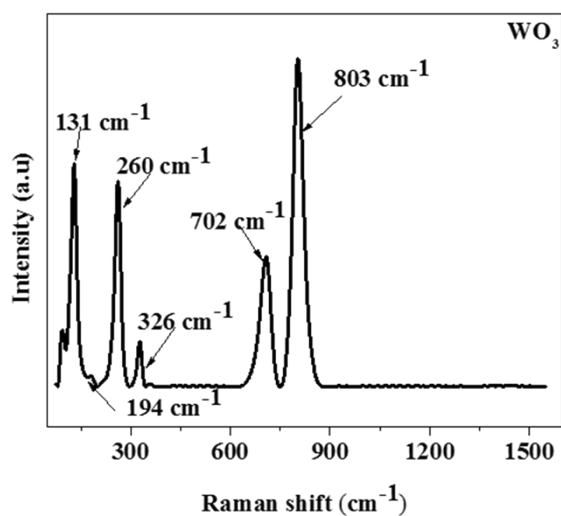
Fig. S6. Laser Raman spectrum of WO_3.

The crystal structure of TiO_2 nanoparticles was also investigated by laser Raman spectroscopy as shown in **Fig. S7**. The Raman active modes observed at 146 cm^{-1}(E_g), 396 cm^{-1}(B_{1g}), 518 cm^{-1}(A_{1g}), and 641 cm^{-1}(E_g) were all typical of the anatase phase of TiO_2, in agreement with PXRD data.
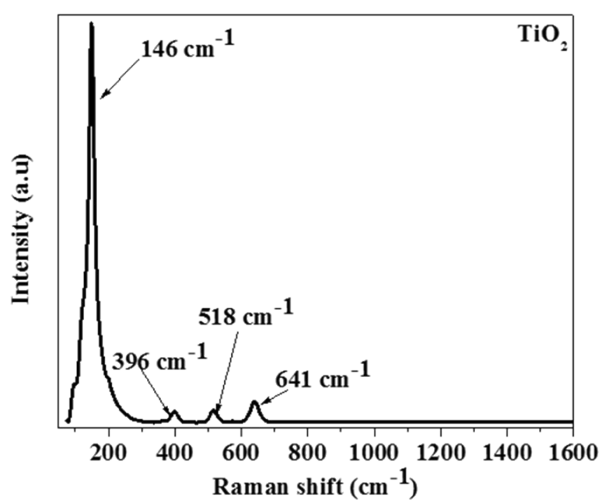
Fig. S7. Laser Raman spectrum of TiO_2.

(S6) PXRD of calcined pure metal oxides

TiO_2 and the QMMOs were calcined at 800 °C in the air to attempt to induce phase changes in the materials. Firstly, the PXRD patterns of pure metal oxides were analyzed (**Fig. S3**). It was observed that the PXRD pattern of ZnO calcined at 800 °C was similar to that of the un-calcined material (**Fig. S8a**), except for that the peaks were sharper indicating improved crystallinity, which typically happens when materials are subjected to higher temperatures.

In the case of WO_3, there was a slight difference observed in the two PXRD patterns (calcined at 800 °C and 400 °C). The disappearance of the (100) reflection at 16 ° was observed when the two patterns were compared (**Fig. S8b**). A similar PXRD pattern was reported by Leghari *et al*., who assigned the pattern as of monoclinic WO_3.[3] Furthermore, Szilagyi *et al*. observed that having calcined hexagonal WO_3 to temperatures beyond 550 °C, it changed into its monoclinic form.[4]

The PXRD pattern of TiO_2 after it had been calcined at 800 °C was totally different from that of TiO_2 before it was calcined (**Fig. S8c**). The reflections were observed at 2θ positions of: 32, 43, 46, 49, 52, 64, 67, 75 and 77 °, indexed as: (110), (101), (111), (211), (220), (002), (311), (301) and (112) (JC JCPDS, no. 21-1276) respectively. The peaks were consistent with those of tetragonal rutile phase.
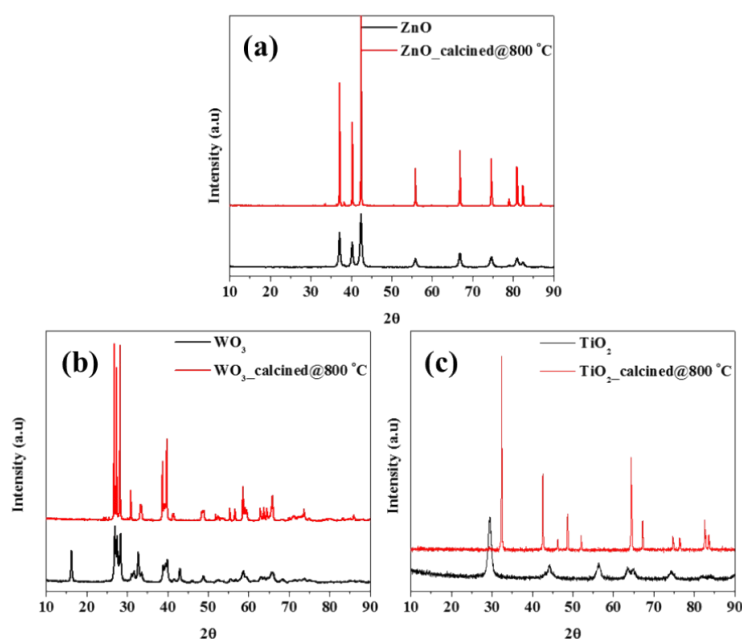
Fig. S8 PXRD patterns of pure metal oxides before (calcined only at 400 °C) and after calcining at 800 °C.

(S7) PXRD of QMMOs supported on NCNTs
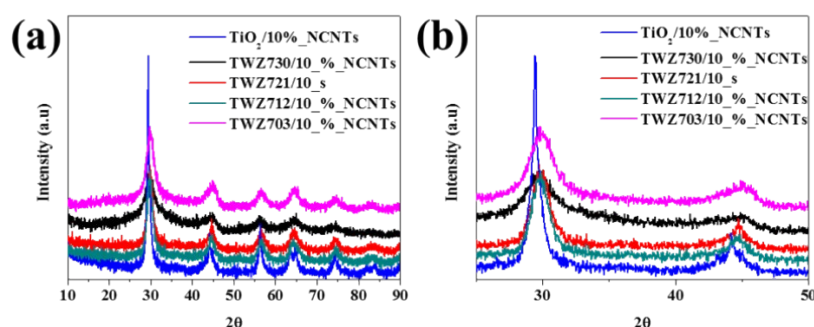
Fig. S9 (a) PXRD patterns of TiO₂/QMMOs and 10 % NCNTs composites and (b) insert showing the (101) reflection.

PXRD analyses were also done on the TiO$_2$/QMMOs and NCNTs composites in order to investigate the crystallographic properties of the materials. The PXRD patterns of the composites were found to be similar to those of TiO$_2$ and QMMOs, suggesting that the addition of NCNTs and the modified synthesis procedure did not alter the formation of QMMOs and TiO$_2$ (**Fig. S3a**). Moreover, the centroid of the (101) reflection of TiO$_2$ was observed at a lower 2θ values relative to those of QMMOs as it was the case with QMMOs (not supported on NCNTs) as shown in **Fig. S3b** This was an indication that even the modified synthesis method yielded QMMOs.

(S8) TGA analyses
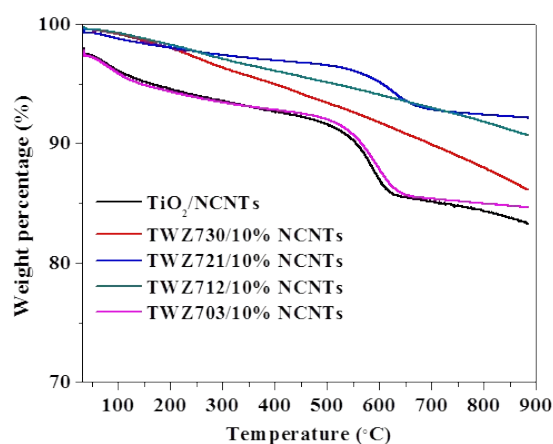
Fig. S10 Thermograms of TiO₂ and QMMOs loaded onto 10 % NCNTs

TGA analyses were conducted on the composites in order to determine if NCNTs were part of the composites as it was observed by TEM (**Fig. 11**). The thermograms showed that the materials were thermally stable with less than 15 % of the material combusting at temperatures between 32 and 900 °C in oxygen (**Fig. S4**). The stability of the materials is typical of metal oxides as they are able to withstand high temperatures

without combusting. The small amount of material (>15 %) was attributed to the NCNTs onto which TiO_2 and the QMMOs were loaded onto. During the synthesis of the samples, 10 % of the materials were NCNTs, the small discrepancies observed on the thermograms were attributed to the inhomogeneity of the samples. Nevertheless, the amounts combusted were estimated to be between 7-14 % of the materials from the thermograms which were close to the pre-calculated 10 %.
(S8)

(S9) Photocatalytic efficiencies
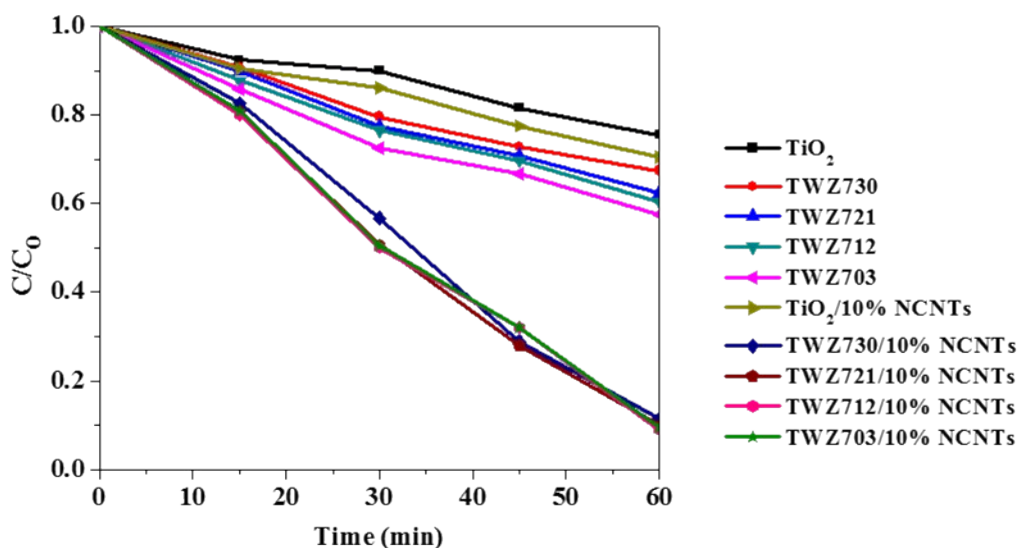
Fig. S11 Photocatalytic efficiencies of TiO_2, QMMOs, and composites.

(S10) Photocurrent measurements
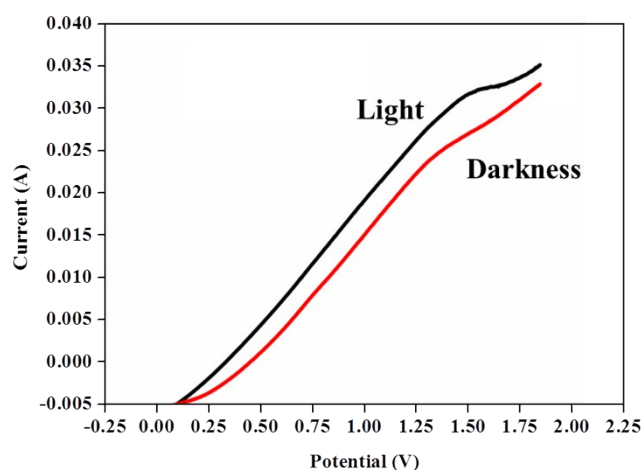
Fig. S12 Linear sweep voltammetry of TWZ712/10% NCNTs.

Linear sweep voltammetric studies of TWZ712/10 % showed the current response over an applied potential range was higher when the photocatalyst was irradiated as opposed when

the measurements were conducted in the dark. Further showing the viability of the material as a photocatalyst.

References

1   L. Hlekelele, P. J. Franklyn, F. Dziike and S. H. Durbach, *New J. Chem.*, 2018, **42**, 1902-1912.

2   L. Hlekelele, P. J. Franklyn, F. Dziike and S. H. Durbach, *New J. Chem.*, 2018, **42**, 4531–4542.

3   S. A. Khan Leghari, S. Sajjad and J. Zhang, *RSC Adv.*, 2014, **4**, 5248-5253.

4   I. M. Szilágyi, S. Saukko, J. Mizsei, A. L. Tóth, J. Madarász and G. Pokol, in *Solid State Sciences*, 2010, **12**, 1857-1860.